

---

# Detection of Crab radiation with a meteorological balloon borne phoswich detector

Ritabrata Sarkar · Sandip K.  
Chakrabarti · Debashis Bhowmick ·  
Arnab Bhattacharya · Abhijit Roy

**Abstract** We use existing light weight balloon facility of Indian Centre for Space Physics to detect the X-ray radiation from Crab pulsar with a phoswich detector. We present the design considerations and characterization of the detector used for this purpose. We model the background radiation in the detector environment at various altitudes and use this in spectral analysis. The background radiation level and limitations on the detector allowed us to calculate minimum detection limit for extrasolar radiation sources with our set up.

**Keywords** X- and  $\gamma$ -ray telescopes and instrumentation · Background radiations · Observation and data reduction techniques; computer modeling and simulation · Astronomical and space-research instrumentation

**PACS** 95.55.Ka · 98.70.Vc · 95.75.-z · 95.55.-n

## 1 Introduction

Indian Centre for Space Physics (ICSP) has been pursuing an independent space program with light-weight meteorological balloons for more than a decade (*Chakrabarti et al.*, 2011, 2013, 2014, 2015, 2017, collectively denoted as *C1117*). In this new paradigm of the space exploration with light weight detectors clearly have merits and difficulties. However, despite their limitations a great deal of science can be done. The payloads used in these ‘Dignity’ series missions

---

This work is partially supported by the Science and Engineering Research Board, India grant number EMR/2016/003870

Ritabrata Sarkar · Sandip K. Chakrabarti · Debashis Bhowmick · Arnab Bhattacharya ·  
Abhijit Roy  
Indian Centre for Space Physics, 43 Chalantika, Garia Station Rd., Kolkata 700084  
Tel.: +91-33-24366003  
Fax: +91-33-24622153  
E-mail: ritabrata.s@gmail.com

are about 5 kg weight containing mainly charge particle or X-ray detectors along with some auxiliary systems. Details of such experimental initiative can be found in *Chakrabarti et al. (2017)*; *Sarkar (2018)* and references therein.

Apart from various constraints, two main challenges to face in this type of experiments are: excess background radiation in the atmosphere and availability of limited time to observe a specific source. The minimum detectability or sensitivity of the detector is limited by both these effects and one has to carefully choose the experimental parameters and conditions to get the highest possible exposure of the source and lowest possible the background. One of the adverse characteristics of using light weight payloads on board single meteorological balloons is that in the absence of ballast and valve systems, the balloon goes up to a certain height, gets ruptured at the burst height and then steadily comes down. Since there is not really a cruising level of the payload, it is always under diverse background environment and at the same time radiation from the (external) source also undergoes different amount of absorption due to the ever changing residual atmosphere.

Moreover, due to the weight constraint on the payload, we cannot deploy a pointing device in the payload to lock the source in the detector direction. Thus the payload is free to rotate about its axis which is along the string attaching the payload to the balloon. The payload is also under local turbulence due to wind pattern and its interaction with the balloon itself. One needs to consider these effects along with the payload altitude during the analysis of the radiation data from the source. These considerations constrain the design of the collimator of the detector to provide an optimum Field of View (FoV) to the detector so that a balance between background counts and exposure time may take place.

The nature of the background noise depends on the payload altitude, observation time and other space weather effects like solar activity etc. and discussed in more details in *Bazilevskaya and Svirzevskaya (1998)*; *Sarkar et al. (2017)* and *C1117*. However, along with the external background we also have to take detector internal background into account (*Peterson, 1975*). The estimation and minimization of the background is particularly important for the observation of astronomical objects which are very faint and the signal-to-noise ratio could be quite poor. In the present work, we demonstrate how modeling of the background radiation could be done using a strong and standard astronomical X-ray source, namely, the Crab pulsar. We use a 5" phoswich scintillator detector for this purpose. Since the discovery of Crab in 1968 by radio telescope (*Staelin & Reifenstein, 1968*) and subsequently in gamma-ray band (*Vasseur et al., 1970*) through balloon-borne experiment, many major astronomical experiments continue to observe the source. Being one of the most powerful extrasolar sources emitting quite stable flux density with stable spectral shape, this source has acted as a standard calibrator. Nevertheless, the source remained a fascinating object to the astronomers and the complete physical processes responsible for its emission still remain to be understood (*Kirsch et al., 2005*; *Vadawale et al., 2017*). In the same spirit, we also choose this source as the candidate for observation to guide us the way the back-

grounds should be eliminated and to validate our new paradigm for X-ray astronomy.

The developmental works of this paradigm are already described in *C1117* and we do not repeat them here. With X-ray detectors, the Dignity series so far has flown 109 missions many of which were to test various modules. In §2, we briefly describe a general mission present the detector design. We discuss detector characteristics such as calibration and resolution and its response functions in §3 and the effects of the residual atmosphere in §4. In §5, we discuss the detector background characteristics at different altitudes and formulate an empirical model to calculate the background and determine the sensitivity of the detector at various altitudes. In §6 we present the results of radiation detection from the Crab pulsar and finally we conclude our work in §7.

## 2 Experiment and instrumentation

A scintillator detector in phoswich combination was flown on board balloon in Dignity mission. The phoswich detector consists a NaI(Tl) crystal of 3 mm thickness and 116 mm diameter. Beneath the NaI crystal there is a 25 cm thick CsI(Na) crystal of same diameter to provide the active background noise cancellation using anticoincidence techniques. The scintillation light produced in the crystals are read out by the Photo-Multiplier Tube (PMT) and their origins are distinguished from the corresponding pulse shape. Similar detectors were used in the RT-2 experiment (*Rao et al.*, 2011) on board CORONAS-PHOTON satellite to study solar activity and other galactic and extra-galactic sources. More details of the detector are in *Debnath et al.* (2011).

The payload with the same detector was redesigned with optimized shielding, collimator and readout system to suit our experimental environment and science goals. We shielded the crystal part with 1 mm tin and 0.2 mm copper underneath to prevent the low energy background where the detector is most sensitive. We put no extra shielding at the lower part containing the PMT due to weight constraints, as the low energy photons from this direction into the detector will first interact in CsI and will be discarded by the anticoincidence logic. The collimator is made of 0.5 mm lead to provide  $\sim 15^\circ$  FWHM FoV. This is the optimum FoV calculated considering the lack of pointing device which could lock the source in the FoV for longer exposure. But since our payload is free to rotate around its axis and susceptible to external jittering, the exposure depends on these rotation and jittering effects and also on the motion of the source (due to earth's rotation) through the detector FoV. So we need to keep the FoV wider to have longer exposure but in turn it reduces the sensitivity of the detector as it allows larger external background. A schematic diagram of the detector along with the collimator and shielding is shown in Fig. 1 (left panel) and the block diagram of the readout scheme is given at the right panel of the same figure.

The detector and the electronic readout system are powered from battery provided in the payload. The signal amplification system is achieved by two

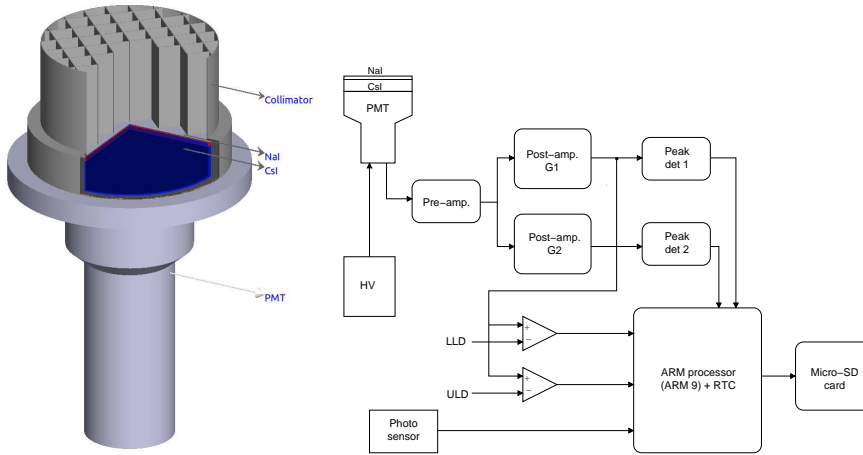


**Fig. 1** (Left:) a schematic diagram of the phoswich detector along with the PMT, collimator and shielding. (Right:) block diagram representation of the electronics and readout system of the detector.

post amplifiers. One (G1) for the low energy part giving  $\sim 15$ -100 keV energy range for most of the radiation sources of our interest which shows significant activity in this energy range. The other post amplifier (G2) can provide energy detection up to  $\sim 2000$  keV to detect other high energy phenomena like TGF etc. In the scope of this current work we will only consider the data from G1. More details of the detector configuration, operation and readout system is described in *Bhowmick et al. (2018)*.

The principal purpose of this experiment is to measure the radiation from the standard astronomical source: Crab pulsar. So we scheduled the date and time of the experiment to have the source inside the FoV of the detector when it is near the top of the atmosphere and without much tilting the viewing axis of the detector from zenith to discard the reduction of effective exposure time due to the payload rotation. The summary of the mission related information are given in Table 1 and more detailed methodology of the experiment and the payload can be found in *Chakrabarti et al. (2017)*.

We show the position of Crab location in altitude angle in the local sky with time and payload altitude in Fig. 2 (only above 30 km). We also plot the detector direction and the sky coverage of the detector FoV at each instant. It is evident from the plot that Crab is inside the FoV for the entire time when the payload is above 30 km and we also calculate the effective area provided by the detector for the position of the source at each instant which is necessary for the spectral analysis of the radiation from the source.

Main detector on board	116 mm diameter phoswich detector with 3 mm NaI and 25 mm CsI crystal.
Collimator	made of 0.5 mm thick lead (15° FWHM FoV).
Other ancillary instruments	GPS system, payload tracker system, attitude measurement system.
Total payload weight	5.7 kg.
Payload carrier	one meteorological plastic balloon (length: $\sim$ 25 m, weight: 7.55 kg).
Date of launch	12 May, 2016.
Time duration	6:12 – 9:13 UT.
Place of launch	Muluk, W.B., India (Lat: 23.6468, Lon: 87.7151).
Maximum height attained	41.05 km (at 7:23 UT).

**Table 1** Mission particulars of the experiment.

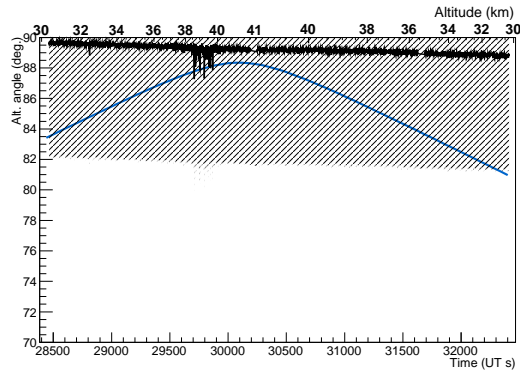


**Fig. 2** Direction of the detector along with sky coverage by the FoV (black) and position of Crab (blue) w.r.t time and altitude above 30 km. The FoV of the detector is shown by the shaded area.

### 3 Detector characteristics

We studied and optimized the detector characteristics for these types of missions through several tests in the laboratory and Monte-Carlo simulations. The details of the laboratory tests done on the detector to study the effect of diverse atmospheric conditions such as temperature, pressure etc. are described in *Chakrabarti et al. (2017)*; *Bhowmick et al. (2018)* and *C1117*.

### 3.1 Calibration and resolution

For calibration of the detector we use laboratory radiation sources: Eu152, Ba133 and Am241 which have several lines inside the sensitive energy range of the detector to give a linear channel-energy relationship. We also calculate the detector resolution at different energies which we find to vary as  $6.62 E^{-0.85}$ . We use this relation for binning of the detector energy range for spectral studies.

### 3.2 Response Matrix Function

The overall response of the detector to the external radiation is divided in two components: the Response Matrix Function (RMF) and Ancillary Response Function (ARF). RMF contains the differential probability of a photon incident on the crystal to be detected in certain energy bin. To generate the RMF of the detector (and for other simulations used in this work) we considered a Monte Carlo simulation of the detector using Geant4 simulation toolkit (version 10.3.1) (Agostinelli *et al.*, 2003) and the energy resolution of the detector at different energies obtained from the laboratory test. For the simulation we considered a flat distribution of  $10^6$  photons in the energy range of 10-100 keV incident on the NaI crystal from above the detector and calculated exclusive energy deposition in NaI crystal only. We modulated the deposited energy in the crystal according to the corresponding resolution of the detector and populated the response matrix. For the electromagnetic interactions of photons in the crystal we considered “em-standard” physics list defined in Geant4. The RMF for the NaI crystal of the detector is shown in Fig. 3.

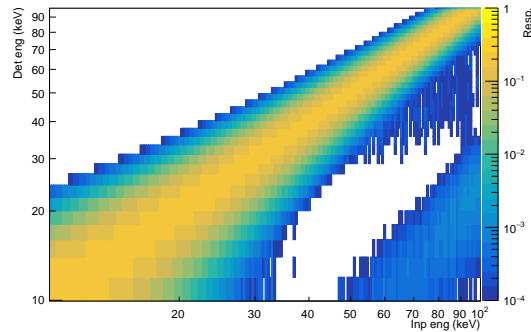


**Fig. 3** RMF of the detector for energy depositions in NaI crystal calculated from simulation and laboratory test.

### 3.3 Ancillary Response Function

The ARF consists of the effective area of the detector for different energies and incident angles. We simulated the detector configuration with proper shielding and collimator with incident photons in the energy range of 10-100 keV from  $4\pi$  solid angle to the detector with random directional distribution. The number of photons entering into the detector will depend on direction of the photons due to position of the crystals and shielding and collimator configuration. The area subtended by the detector crystal also change with the incident angle. Considering these, we calculate the effective area (which also includes the efficiency) of the detector and generate a 3 dimensional matrix with these information for different energies, altitude angle ( $\theta$ ) and azimuth angle ( $\phi$ ). The ARF information for various energies at different  $\theta$  is shown in Fig. 4 in the left panel while the same information for  $\theta = 0^\circ$  is plotted at the right panel.

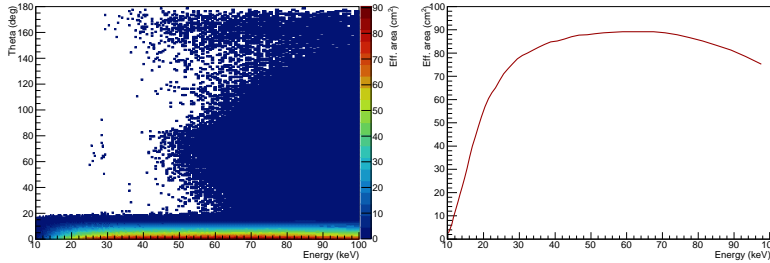


**Fig. 4** (Left:) Effective area distribution of the detector at different  $\theta$  w.r.t energy. (Right:) Effective area plot at  $\theta = 0^\circ$ .

## 4 Atmospheric response

There remains a residual atmosphere at the balloon height causing the absorption and modification of radiation spectrum of the extraterrestrial sources. These must be taken into account to obtain the actual source spectrum. Moreover from Fig. 2 we see that the detector undergoes different amounts of residual atmosphere due to time dependent payload altitude. So, for the spectral analysis with longer exposure time we must dynamically correct for this atmospheric absorption effect. For this purpose we generated a response matrix function and absorption function for the residual atmosphere using Geant4 simulation.

To define the atmosphere we considered the NRLMSISE-00 standard atmospheric model parameters (*Picone et al.*, 2002) with parallel layers of 1 km thickness up to 50 km. We used incident photons in the energy range 10-100 keV perpendicular to the layers from the top of the atmosphere and calculated

the response function and the absorption function at various altitudes up to 42 km. An example of the response and absorption functions at an altitude of 38 km is shown in Fig. 5 for normal incidence of radiation. However depending on the source position, the incident angle ( $\theta_i$ ) may vary and the absorption will be affected by this angle and for larger angles the flat atmospheric layer approximation will fail. But for small incident angles (like  $\leq 15^\circ$  in this case which is limited by the FoV of the detector) the absorption may be approximated to vary as  $1/\cos\theta_i$ . We need to use these atmospheric response and absorption functions in addition to the detector response for the analysis of external radiation.

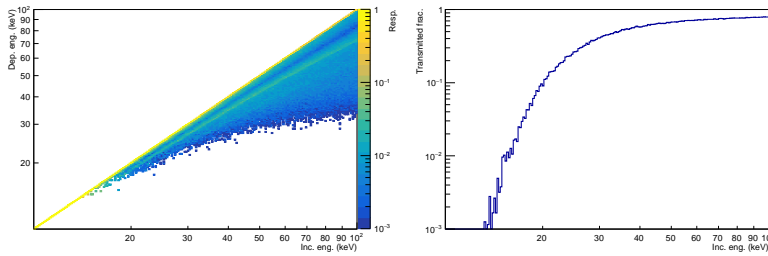


**Fig. 5** (Left:) Atmospheric response matrix for the residual atmosphere at an altitude of 38 km. (Right:) Transmission fraction for photons of different energies at the same altitude.

## 5 Background calculation

The sensitivity of the detector in these types of experiments is highly affected by the atmospheric background due to Cosmic Ray (CR) interactions apart from the primary cosmic background and those which are intrinsic to the detector. Extensive calculations of background noise for a similar detector was done by *Sarkar et al.* (2011) for experiments in satellite environment. In the present experiment, the situation is different due to the presence of atmosphere which makes the computation more complicated. But the fact of not having much high-Z material in the vicinity of the detector means less secondary background from the payload is produced.

There is also a specific problem for these types of experiments regarding the background estimation which one has to overcome. We cannot have actual measurement of simultaneous background when the source is inside the detector for a long time. In this case we must rely on the accurate modelling of the background in that condition. This background has an external part which contains cosmic rays and secondary radiations due to their interaction with the atmosphere. The other part of the background, intrinsic to the detector may again depend on the external background flux and is caused by the activation and spallation of the detector materials. The primary and secondary CR back-

ground depends on the geomagnetic latitude and altitude of the experiment. This CR background on the other hand modulated by space environment condition mainly due to solar activity and is discussed in (*Sarkar et al., 2017*) for similar latitude and energy range.

### 5.1 Trigger efficiency for background components

The external background components at the balloon flight altitude consist of charged particles (protons, alpha, electrons, positrons) and gamma-rays in the cosmic-ray flux and muons from the atmospheric interactions of the primary CRs. *Mizuno et al. (2004)* provides an extensive discussions on the energy dependent flux of these components and their atmospheric depth and angular dependency at the balloon height.

We simulated our detector to calculate the trigger efficiency for each of the external background components distributed in  $4\pi$  solid angle of the detector. The trigger efficiency of the detector (for incident energy range 10 keV - 100 MeV) and the integrated background flux in the energy range of 10-100 keV due to various background components at a height of 38 km is given in Table 2. From the calculation we notice that the most effective component of the background is due to gamma-ray for this type of payloads. The other particles produce negligible trigger in the detector due to thin primary crystal and rejection due to anti-coincidence technique and therefore we do not take them into account. Moreover, the primary gamma-ray flux in CR is less than one order in magnitude to that of the downward secondary photons produced in atmosphere (*Mizuno et al., 2004*), so we consider only secondary gamma-ray in the atmosphere as the principal background source.

Bkg. comp.	Trg. eff.	Int. flux
Gamma	0.174	0.54
Proton	$1.8 \times 10^{-5}$	$7 \times 10^{-6}$
$e^-$	$6.9 \times 10^{-4}$	$3 \times 10^{-3}$
$e^+$	$6.6 \times 10^{-4}$	$4 \times 10^{-3}$
$\mu^-$	$1.9 \times 10^{-3}$	$4 \times 10^{-5}$
$\mu^+$	$2.9 \times 10^{-4}$	$1 \times 10^{-5}$

**Table 2** Trigger efficiency (for incident particles in energy range in 10 keV - 100 MeV) and integral flux (counts/cm<sup>2</sup>/s) in the detector in the energy range of 10-100 keV for various cosmic-ray background components.

### 5.2 Detector background modelling

From Fig. 2 we see that above 30 km the Crab was inside the FoV of the detector. So there is no other way to directly measure the simultaneous back-

ground and we need to rely on the calculated background of the detector. For this reason we developed an empirical model of the detector background. For residual atmosphere less than  $100 \text{ g cm}^{-2}$  the downward secondary gamma-ray flux is proportional to atmospheric depth and upward flux is almost constant (Thompson, 1974). So we considered to fit the detector backgrounds from 20 km ( $55.8 \text{ g cm}^{-2}$ ) till 30 km in each layer of 1 km with the empirical model and extrapolate the model parameters for higher altitudes to calculate the corresponding background.

For external background due to downward and upward secondary gamma-rays we consider the flux distribution according to the power law (Mizuno et al., 2004):

$$A \left( \frac{E}{\text{keV}} \right)^{-1.34} \text{ counts } s^{-1} m^{-2} sr^{-1} keV^{-1} \quad (1)$$

where the flux normalization  $A$  varies with the atmospheric depth and depends on the geomagnetic latitude of the experiment and solar activity. The zenith angle dependence of the flux was taken into account as described in Mizuno et al. (2004).

There are several background sources which are fundamentally internal to the detectors due to radio activity stimulated by CRs (Gruber et al., 1996). Lines coming from K X-ray at 25-30 keV from spallation of tellurium, 58 keV inelastic scattering gamma in iodine are clearly present in the background spectrum.

We fitted the detector background using Equation 1 convoluted by the detector response for different incident angles with one Gaussian to account for the low energy noise near  $\sim 12 \text{ keV}$  and two additional Gaussian lines around 30 and 60 keV. We extracted the model parameters for different atmospheric depths and fitted their variations. We found the flux normalization  $A$  to vary exponentially with atmospheric depth while other parameters vary linearly. In Fig. 6 we show the comparison of the detector background and the modelled background at 30 km height. Using these parameters we are able to calculate the background at higher altitudes when Crab is inside the detector FoV.

### 5.3 Sensitivity of the detector

From the background flux in the detector we calculate the minimum detectable limit or sensitivity of the detector at various altitudes in the atmosphere. In Fig. 7 we have shown, for example, the sensitivity of the detector at three different altitudes of 30, 36 and 40 km. This calculation is done considering 5 minutes of detector exposure time and signal-to-noise ratio of 3 which corresponds to about 99.8% confidence level. The sensitivity is expressed in units of Crab radiation flux modified by the residual atmosphere at that altitude. The calculation affirms that detection of extrasolar sources with Crab like spectrum and a few hundred mCrab flux are possible in a limited hard X-ray energy range.

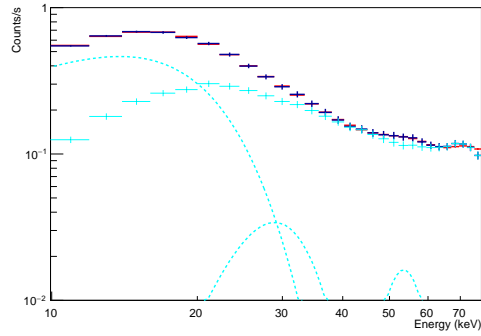


**Fig. 6** Detector background at 30 km (red) and the calculated background according to the empirical model (blue). The model components are shown (in cyan) which consist of three Gaussian (dashed line) for intrinsic background and a power law component for external secondary gamma-ray modified by the detector response (see text for details).

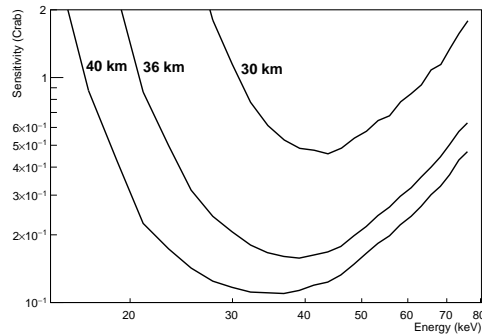


**Fig. 7** Detector sensitivity with energy in units of Crab radiation flux calculated at three different heights of 30, 36 and 40 km.

## 6 Crab data analysis

The radiation flux detected in the entire mission flight in the energy range of 25-60 keV is shown in Fig. 8. In the light curve the first and last peaks are from atmospheric radiation at Regener-Pfotzer maximum due to secondary cosmic rays and has been discussed in *Sarkar et al.* (2017). The peak at the middle is due to the radiation from Crab pulsar and is evident from Fig. 2. There is a little dip in the light curve at around 29 ks which is due to turbulence in the carrier during the balloon rupture and has been confirmed from the camera installed on the payload and from its attitude measurement.

For the spectral analysis of the radiation from the Crab we considered a total of 1178s exposure data which spanned in the altitude range of 38-41 km. For the background data we used the calculated data described in §5.2. We

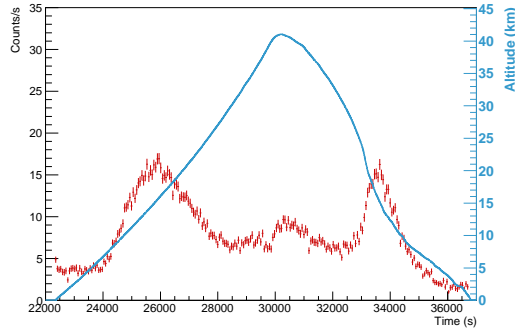


**Fig. 8** 25-60 keV light curve of the overall mission data showing the radiation from Crab above 30 km. Payload altitude is plotted simultaneously to show the detector position.

considered a weighted average of the background in each layer (of 1 km) in the altitude range according to the time taken by the payload to cross each layer.

The Crab spectrum is fitted by the absorbed power-law model (*Kirsch et al.*, 2005):

$$S(E_i) = A E_i^B \exp(-0.38\sigma(E_i)) \quad (2)$$

where,  $S(E_i)$  is in units of photons/cm<sup>2</sup>/s/keV and  $\sigma(E_i)$  is H column cross-section in units of cm<sup>2</sup>. This source spectrum is modified by the atmospheric absorption function ( $A_{abs}(E_i)$ ), atmospheric response function ( $A_{rsp}(E_i, E_a)$ ), detector ARF ( $D_{arf}(E_a)$ ) and detector RMF ( $A_{rsp}(E_a, E_d)$ ) to fit the detected source spectrum  $F(E_d)$ .

$$F(E_d) = A_{rsp}(E_a, E_d) \cdot D_{arf}(E_a) \cdot A_{rsp}(E_i, E_a) \cdot A_{abs}(E_i) \cdot S(E_i) \quad (3)$$

The best fit of the spectrum in the energy range of 20-75 keV gives  $A = 12.36 \pm 4.66$  photons/cm<sup>2</sup>/s/keV and  $B = -2.41 \pm 0.10$  with  $\chi^2 = 26.12$  for 23 NDF. The detected spectrum of Crab radiation along with the calculated background and the model fit is plotted in Fig. 9.

## 7 Conclusions

Indian Centre for Space Physics, through its Dignity missions, has been exploring near space using meteorological balloons for a decade (e.g., *Chakrabarti et al.* (2014, 2015, 2017); *Sarkar et al.* (2017)) and preliminary studies suggest that a great deal of valuable scientific experiments could be carried out with these low-cost Missions. However, unlike experiments with larger balloons and massive payloads, where pointing to a target is possible to raise exposure time and the signal to noise ratio, in our case, pointing is not done explicitly and each photon is tagged with an attitude from which source information is obtained through post-processing. Otherwise corrections due to atmospheric effects and background radiation remain a concern for both the cases.

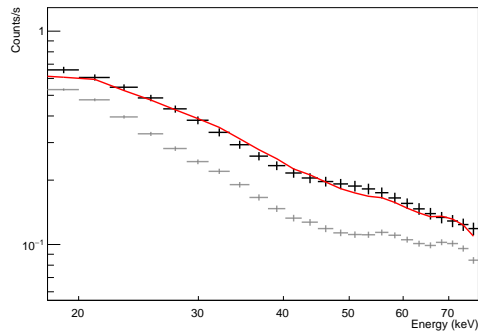


**Fig. 9** The spectrum of Crab radiation (source + background) as seen by the detector (black) along with the calculated detector background (gray). The spectrum is fitted by using an absorbed power law modified by the atmospheric and detector responses.

In the present paper, we went into details of how to eliminate effects of background radiation while studying cosmic X-ray sources. For a case study, we chose a strong and steady X-ray source, namely, the Crab pulsar and show that by systematically eliminating the background noise we recover the spectrum very well. We computed the limit on the sensitivity of the detector. We presented the techniques to estimate the detector characteristics and also estimated the environmental effects on the experiment, such as, the effects of the residual atmosphere. Presently, we find that sources with brightness at ten per cent level as that of the Crab may also be detected by these low-cost missions. However, the sensitivity could be increased further by using lighter detectors with larger area and using better shielding and collimation.

**Acknowledgements** The authors would like to thank the ICSP balloon team members, namely, Mr. S. Midya, Mr. H. Roy, Mr. R. C. Das and Mr. U. Sardar for their dedications during the crucial mission operations such as launching and recovery. This work been done under partial financial support from the Science and Engineering Research Board (Science and Engineering Research Board, Department of Science and Technology, Government of India) project no. EMR/2016/003870. We also thank Ministry of Earth Sciences (Government of India) for partial financial support.

## References

- Agostinelli S., et al.: Geant4 - a simulation toolkit. *Nucl. Instr. Methods, A*, 506, 250–303, (2003).
- Bazilevskaya, G. A., and Svirzevskaya, A. K.: On the stratospheric measurements of cosmic rays. *SpScR*, 85, 431–521, (1998).
- Bhowmick, D., Chakrabarti, S. K. Sarkar, R., Bhattacharya, A. & Rao, A. R.: Development of Instruments for Space Exploration Using Meteorological-balloons. Submitted in *JATIS*, (2018).

- Chakrabarti, S. K., Bhowmick, D., Sarkar, R., Mondal, S., Sen, A.: High Energy Astrophysics with Rubber Balloons, *Proceedings of European Rocket and Balloon Programmes and Related Research*, L. Ouweland (Ed.), ESA SP 711, 581, (2011)
- Chakrabarti, S. K., Bhowmick, D., Palit, S., Chakraborty, S. Mondal, S., Bhattacharyya, A., Middy, S., Chakrabarti, S.,: A New Paradigm in Space Based Experiments Using Rubber Balloons, *Proceedings of European Rocket and Balloon Programmes and Related Research*, L. Ouweland (Ed.), ESA SP 721, 663, (2013)
- Chakrabarti, S. K., Bhowmick, D., Chakraborty, S., Palit, S., *Ind. J. Phys.*, 88, 333, (2014), DOI 1007/s12648-13-0424-z.
- Chakrabarti, S. K., Bhowmick, D., Sarkar, R., Bhattacharyya, A. & Midya, S.: Study of properties of cosmic rays and solar X-ray flares by balloon borne experiments. *Proceedings of European Rocket and Balloon Programmes and Related Research*, L. Ouweland (Ed.), ESA SP 730, 557, (2015).
- Chakrabarti, S. K., Sarkar, R., Bhowmick, D., & Bhattacharyya, A.: Study of high energy phenomena from near space using low-cost meteorological balloons. *Exp. Astron.*, 43(3), 311-338, (2017), DOI 10.1007/s10686-017-9540-7.
- Debnath, D., Nandi, A., Rao, A. R., Malkar, J. P., Hingar, M. K., Kotoch, T. B., Sreekumar, S., Madhav, V. P., Chakrabarti, S. K.: Instruments of RT-2 experiment onboard CORONAS-PHOTON and their test and evaluation I: ground calibration of RT-2/S and RT-2/G. *Exp. Astron.*, 29(1-2), 1-25, (2011).
- Gruber, D. E., Blanco, P. R., Heindl, W. A., Pelling, M. R., Rothschild, R. E., Hink, P. L.: The high energy X-ray timing experiment on XTE.. *A&AS*, 120, 641-644, (1996).
- Kirsch, M. G. et al.: Crab: the standard X-ray candle with all (modern) X-ray satellites. *UV, X-Ray, and Gamma-Ray Space Instrumentation for Astronomy XIV. Proceedings of the SPIE* 5898, 22-33, (2005).
- Mizuno, T., Kamae, T., Godfrey, G., Handa, T., Thompson, D. J., Lauben, D., Fukazawa, Y., Ozaki, M.: Cosmic-Ray Background Flux Model Based on a Gamma-Ray Large Area Space Telescope Balloon Flight Engineering Model. *ApJ*, 614, 1113-1123, (2004).
- Peterson, L. E. 1975, Instrumental technique in X-ray astronomy, *ARA&A* 13, 423-509.
- Picone, J. M., Hedin, A. E., Drob, D. P., and Aikin, A. C.: NRL-MSISE-00 Empirical Model of the Atmosphere: Statistical Comparisons and Scientific Issues. *JGR*, 107, A12, 1468, (2002)
- Rao, A. R., Malkar, J. P., Hinger, M. K., et al.: Onboard performance of the RT-2 detectors. *SoSyR*, 45(2), 123-134, (2011).
- Sarkar, R., Mandal, S., Debnath, D., Kotoch, T. B., Nandi, A., Rao, A. R., Chakrabarti, S. K.: Instruments of RT-2 experiment onboard CORONAS-PHOTON and their test and evaluation IV: background simulations using GEANT-4 toolkit. *Exp. Astron.*, 29(1-2), 85-107, (2011).

- Sarkar, R., Chakrabarti, S.K., Pal, P.S., Bhowmick, D. and Bhattacharyya, A.: Measurement of secondary cosmic ray intensity at Regener-Pfotzer height using low-cost weather balloons and its correlation with solar activity. *AdvSpRes*, 60, 991-998, DOI 10.1016/j.asr.2017.05.014, (2017).
- Sarkar, R.: Detector Development and Optimization for Space Based Astronomy from Satellites and Balloons. In *Exploring the Universe: From Near Space to Extra-Galactic, Astrophysics and Space Science Proceedings*, 53, pp. 371, Springer International Publishing AG, part of Springer Nature, (2018).
- Staelin, D. H., Reifenstein, E. C., III: Pulsating Radio Sources near the Crab Nebula. *Science*, 162, 1481-1483, (1968)
- Thompson, D. J.: A three-dimensional study of 30- to 300-MeV atmospheric gamma rays. *J. Geophys. Res.*, 79, 1309-1320, (1974).
- Vadawale, S. V., Chattopadhyay, T., Mithun, N. P. S., et al.: Phase-resolved X-ray polarimetry of the Crab pulsar with the AstroSat CZT Imager. *Nature Astron.*, 2(1), 50-55, (2017).
- Vasseur, J., Paul, J., Parlier, B. et al.: Possible Pulsed Gamma Ray Emission above 50 MeV from the Crab Pulsar. *Nature*, 226, 534-535, (1970).